Int. J. Solids Structures, 1971, Vol. 7, pp. 731 to 750. Pergamon Press. Printed in Great Britain

TRANSIENT STRESS INTENSITY FACTORS FOR A FINITE CRACK IN AN ELASTIC SOLID CAUSED BY A DILATATIONAL WAVE†

STEPHEN A. THAU‡ and TSIN-HWEI LU§

Department of Mechanics, Illinois Institute of Technology, Chicago, Illinois

Abstract—The diffraction of a plane dilatational wave of arbitrary profile by a finite line crack in an infinite elastic medium is analyzed by the generalized Wiener–Hopf technique. Explicit expressions are derived for the dynamic normal and shear stress intensity factors at each crack edge as functions of time, angle of incidence and Poisson's ratio. These results are exact from the instant the incident wave arrives at a given edge until a diffracted P wave reaches the opposite edge, is rediffracted, and then returns to the original edge, i.e. during two P wave, crack width transit times. Numerical results for an incident wave with a step function stress profile are presented for several angles of incidence and the peak normal stress intensity is found to be 30 per cent greater than the analogous static factor. The magnitude of the jump in the vertical displacement across the crack is also calculated for the case of normal incidence, during a single P wave transit time and the crack is found to remain open in this period.

1. INTRODUCTION

THE calculation of stresses around a crack in an elastic medium is a problem of long-standing interest in fracture mechanics. For the case of time-harmonic dynamic loading, Sih and Loeber have recently obtained results for the stress intensities at the edges of a finite crack subjected to a plane incident stress wave [1]. They treated both harmonic dilatational (P wave) and vertical shear (SV wave) waves and in an earlier paper they considered an incident, harmonic, horizontal shear wave (SH wave) [2].

In this paper we treat the analogous *transient* problem of diffraction of an arbitrary plane dilatational wave by a finite crack in an infinite elastic solid. As done in our previous study on the diffraction of a plane transient SH wave by a finite crack [3], we employ the so-called generalized Wiener–Hopf method which yields an iteration series solution that is exact for a finite period of time which increases with each increasing order of the iteration. This technique has also been used by us [3], Kostrov [4] and Flitman [5], in problems of diffraction of elastic waves by a finite rigid strip. We are again successful here in obtaining explicitly zeroth and first order expressions for the stress intensity factors. The first order results are exact from the time the incident wave reaches the crack until two P wave, crack width transit times have elapsed. The peak stress intensity factors are found to occur at the instant when the first scattered Rayleigh waves, which propagate along the crack surfaces, arrive at the given crack edge. For later times than considered here, the exact generalized Wiener–Hopf iteration solution is no longer practical for calculating numerical

† This research was supported by a National Science Foundation Grant No. GK 1911 to the Illinois Institute of Technology.

‡ Associate Professor.

§ Research Assistant.

results. However, in all the cases cited above, including the present study, peak responses are found to occur in the time period of two crack or rigid strip transit times.

The application of the Wiener–Hopf method for the finite strip or slit diffraction problem is discussed in chapter V of Noble's book [6], but only for high-frequency scalar harmonic waves and for far-field calculations. Then the results are asymptotic rather than exact.

2. DESCRIPTION OF PROBLEM

The infinite elastic solid shown in Fig. 1 contains a plane crack of unit width and infinite length situated at $y = 0$ and $0 < x < 1$.† A plane transient compressional wave impinges on the crack with its propagation vector perpendicular to the z-axis and at an angle α from the positive x-axis. The problem is therefore taken as one of plane strain in which the displacements are independent of z and can be expressed in terms of the compressional (P wave) and shear (S wave) wave potentials, $\phi(x, y, t)$ and $\psi(x, y, t)$, respectively, as

$$u = \partial\phi/\partial x + \partial\psi/\partial y,\ v = \partial\phi/\partial y - \partial\psi/\partial x,\ \omega = 0 \tag{1}$$

With dots over a function indicating differentiation with respect to time, the equations of motion become

$$\nabla^2\phi - \ddot{\phi} = 0, \qquad \nabla^2\psi - \kappa^2\ddot{\psi} = 0 \tag{2}$$

where

$$\kappa = [(2-2\nu)/(1-2\nu)]^{\frac{1}{2}} \tag{3}$$

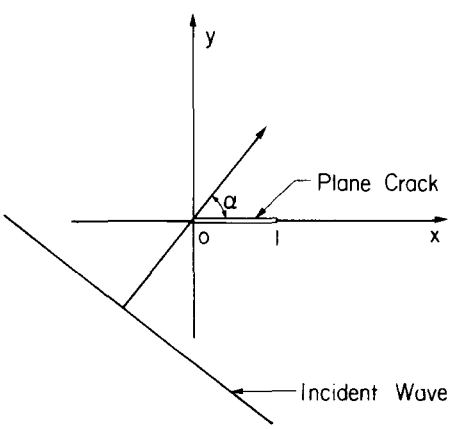

FIG. 1. Geometry of problem.

† The Cartesian coordinates x, y, z have been normalized by the actual physical width of the crack. Also, the dimensionless time adopted here is equal to the actual time normalized by the time for a P wave to transverse the width of the crack. Hence, in these dimensionless coordinates, the P and S wave velocities become unity and $1/\kappa$ (< 1), respectively.

is the ratio of the P wave velocity to the velocity of the S wave.† Note that for real elastic solids for which the Poissons ratio ν is in the range $0 < \nu < \frac{1}{2}$, $\kappa > 2^{\frac{1}{2}}$. The stresses in the medium, normalized by the shear modulus, are calculated from Hooke's law as

$$\tau_{ij} = u_{i,j} + u_{j,i} + (\kappa^2 - 2)\delta_{ij} u_{k,k} \tag{4}$$

in Cartesian tensor notation.

The incident wave, indicated with superscript (i), is given by

$$\phi^{(i)} = f(t - x\cos\alpha - y\sin\alpha), \qquad \psi^{(i)} = 0 \tag{5}$$

where f is identically zero when its argument is negative, but otherwise is an arbitrary waveform. Thus the initial time for the problem is the instant when the wave (5) reaches the leading edge of the crack, $x = 0$. Ahead of the advancing plane front the medium is undisturbed.

The stresses produced by the incident wave are

$$\tau_{xx}^{(i)} = (\kappa^2 - 2\sin^2\alpha)\ddot{f}, \qquad \tau_{yy}^{(i)} = (\kappa^2 - 2\cos^2\alpha)\ddot{f} \qquad \tau_{xy}^{(i)} = \sin 2\alpha\, \ddot{f}. \tag{6}$$

In the numerical example in Section 5, $\ddot{f}$ is taken as the unit step function. Then in the long time limit the incident stress wave field becomes a biaxial state of static tension of magnitude κ^2 at an angle α from the positive x-axis and of magnitude $(\kappa^2 - 2)$ in the perpendicular direction. Thus, at large times the dynamic crack-tip, stress intensity factors should approach the static ones produced by this biaxial loading.

The scattered waves (s) which are added to the incident waves to form the total field are determined from equation (2) and the boundary conditions

$$\begin{aligned} \tau_{yy}^{(s)} &= -\tau_{yy}^{(i)} \quad \text{at } y = 0, \qquad 0 < x < 1 \\ \tau_{xy}^{(s)} &= -\tau_{xy}^{(i)} \quad \text{at } y = 0, \qquad 0 < x < 1 \end{aligned} \tag{7}$$

which specify that the crack surfaces are separated and free of traction.‡ Also to guarantee a unique solution we require that the displacements be finite at the edges of the crack and that the scattered waves are outgoing.

3. SOLUTION OF PROBLEM

To begin the analysis of the problem we decompose the incident wave into even and odd functions of y as

$$\phi^{(i)} = \phi_e^{(i)} + \phi_0^{(i)} \tag{8}$$

where

$$\phi_{e,0}^{(i)} = \tfrac{1}{2} f(t - x\cos\alpha - y\sin\alpha) \pm \tfrac{1}{2} f(t - x\cos\alpha + y\sin\alpha) \tag{9}$$

† The Cartesian coordinates x, y, z have been normalized by the actual physical width of the crack. Also, the dimensionless time adopted here is equal to the actual time normalized by the time for a P wave to transverse the width of the crack. Hence, in these dimensionless coordinates, the P and S wave velocities become unity and $1/\kappa$ (< 1), respectively.

‡ This assumption is examined in Section 4.

and then treat the scattering problems for the even and odd incident waves separately. From the geometry it follows that in the symmetric problem (involving $\phi_e^{(i)}$) ϕ, u, τ_{xx} and τ_{yy} will be even functions of y for both the incident and scattered waves, while ψ, v and τ_{xy} will similarly be odd in y. In the anti-symmetric problem (with $\phi_0^{(i)}$) the even and odd conditions for these fields are reversed. For each problem we need consider only the half-space region $y > 0$.

(a) *Symmetric problem*

In the symmetric problem the incident P wave is given by equations (9) with the upper sign. It produces zero shear stress and normal displacement along $y = 0$ and generates the normal stress at $y = 0$

$$\tau_{yy}^{(i)}(x, 0, t) = \Gamma_1 \ddot{f}(t - x\cos\alpha) \tag{10}$$

with $\Gamma_1 = \kappa^2 - 2\cos^2\alpha$. Furthermore, since the scattered wave field is continuous at $y = 0$, except possibly along the crack where it may jump, we know that $v^{(s)}$ and $\tau^{(s)}$ will be zero at $y = 0$ for $x < 0$ and $x > 1$. Hence, from equation (7) $\tau_{xy}^{(s)}$ is known along the entire x-axis and by introducing specific functions to be determined for the unknown boundary values of $v^{(s)}$ and $\tau_{yy}^{(s)}$ along $y = 0$, we can extend conditions (7) to

$$v^{(s)}(x, 0^+, t) = \begin{cases} \kappa^2 g(x, t)/2(\kappa^2 - 1) & \text{for } 0 < x < 1 \\ 0 & \text{otherwise} \end{cases} \tag{11a}$$

$$\tau_{xy}^{(s)}(x, 0, t) = 0 \quad \text{for all } x \tag{12a}$$

$$\tau_{yy}^{(s)}(x, 0, t) = \begin{cases} \dot{\tau}_0(x, t) & \text{for } x < 0 \\ -\Gamma_1 \ddot{f}(t - x\cos\alpha) & \text{for } 0 < x < 1 \\ \dot{\tau}_1(x - 1, t) & \text{for } 1 < x \end{cases} \tag{13a}$$

where the factor $\kappa^2/2(\kappa^2 - 1)$ in equation (11a) and the time derivatives of τ_0 and τ_1 in equation (13a) are introduced for convenience in subsequent algebraic manipulations. We take g, τ_0 and τ_1 to be identically zero along the x-axis outside the respective intervals where they do not define boundary data for the scattered wave field.

Physically, since the incident wave is continuous everywhere, $\kappa^2 g(x, t)/(\kappa^2 - 1)$ is the total jump in the vertical displacement along the crack. We shall calculate this function in Section 4. Also, $\dot{\tau}_0$ and $\dot{\tau}_1$ contain the total dynamic crack-tip, stress-intensity factors for the normal stresses at the tips $x = 0$ and 1, respectively.†

To solve equations (2) for the scattered waves we employ the Wiener–Hopf method. First the Laplace transform in t and the Fourier transform in x are applied to the complete set of governing equations. The Laplace transform is indicated with an overbar as

$$\bar{f}(s) = \int_0^\infty f(t)\, e^{-st}\, dt \tag{14}$$

† Recall that v is an even function and hence continuous at $y = 0$ in the anti-symmetric problem, while τ_{xx} and τ_{yy} are odd functions and thus vanish at $y = 0$ for $x < 0$ and $x > 1$. The total jump in the horizontal displacement along the crack and the shear stress intensity factors are provided by the solution of the anti-symmetric problem in Sub-section (b), below.

where s may be treated as a positive real parameter throughout the analysis. The Fourier transform is specified by the corresponding upper case letter as

$$F(\zeta s) = \int_{-\infty}^{\infty} f(x)\, e^{-i\zeta s x}\, dx \tag{15a}$$

where the Fourier transform parameter is taken as ζs ($\zeta = \xi + i\eta$) instead of ζ, again for convenience in subsequent algebraic calculations. Thus the inverse Fourier transform becomes

$$f(x) = \frac{s}{2\pi} \int_{-\infty + ic}^{\infty + ic} F(\zeta s)\, e^{i\zeta s x}\, d\zeta \tag{15b}$$

where c is any constant that places the line $\xi + ic$ ($-\infty < \xi < \infty$) in a region of the ζ-plane where $F(\zeta s)$ is an analytic function.

In applying the Laplace transform, we recall from the definition of the initial time for the problem, that zero initial conditions hold for the scattered waves. Thus, the appropriate doubly transformed solutions of equations (2) in $y > 0$ become

$$\bar{\Phi} = A\, e^{-\alpha s y}, \qquad \bar{\Psi} = B\, e^{-\beta s y} \tag{16}$$

with

$$\alpha^2 = \zeta^2 + 1, \qquad \beta^2 = \zeta^2 + \kappa^2. \tag{17}$$

To render α and β single-valued, the usual branch cuts are taken in the ζ-plane along the imaginary axis: from $\eta = 1$ to ∞ and $\eta = -1$ to $-\infty$ for α and $\eta = \kappa$ to ∞ and $\eta = -\kappa$ to $-\infty$ for β.

Next, the doubly transformed boundary conditions along $y = 0$ are found to be

$$\bar{V}^{(s)} = \kappa^2 \bar{G}_E / 2(\kappa^2 - 1) \tag{11b}$$

$$\bar{\Upsilon}_{xy}^{(s)} = 0 \tag{12b}$$

$$\bar{\Upsilon}_{yy}^{(s)} = s\left[\bar{\Upsilon}_+ + e^{-i\zeta s}\bar{\Upsilon}_- + \frac{i\Gamma_1 \bar{f}}{\zeta - i\cos\alpha}\,(1 - e^{-s\cos\alpha - i\zeta s})\right] \tag{13b}$$

where the $+$, $-$ and E subscripts refer to regions in the ζ-plane in which the various Fourier transforms are known to be analytic functions. The $+$ and $-$ regions are the overlapping half-planes $\eta > -1$ and $\eta < 1$, respectively, while the E region is the entire ζ-plane. They are determined as follows: since $\bar{\tau}_0(x, s)$ and $\bar{\tau}_1(x-1, s)$ represent outgoing waves emanating from the crack tips $x = 0, 1$, respectively, they will contain the exponential factors $\exp(sx)$ and $\exp(s - sx)$, respectively. Thus, the Fourier transform integral for $\bar{\tau}_0$ converges and hence is analytic in the $+$ region, $\eta > -1$, while that for $\bar{\tau}_1$ converges in the $-$ region, $\eta < 1$. Furthermore, the Fourier transform of $\bar{g}(x, s)$ is a proper integral and so it converges to an analytic function in the entire ζ-plane. Note that, because the apparent pole at $\zeta = i\cos\alpha$ in equation (13b) is actually a removable one and from the choice of branch cuts for α and β, all the Fourier transforms are analytic in the overlap strip $|\eta| < 1$.

By substitution of equations (16) into the transforms of equations (1) and (4) and then into equations (11b)–(13b) we obtain three equations for the five unknowns A, B, $\bar{G}_E$, $\bar{\Upsilon}_+$ and $\bar{\Upsilon}_-$. Elimination of A and B from these equations yields the generalized Wiener–Hopf equation:

$$-\bar{G}_E\alpha^{-1}(\zeta^2+\gamma^2)K(\zeta) = \bar{\Upsilon}_+ + e^{-i\zeta s}\bar{\Upsilon}_- + \frac{i\Gamma_1\bar{f}}{\zeta - i\cos\alpha}(1-e^{-s\cos\alpha - i\zeta s}) \tag{18}$$

where

$$K(\zeta) = R(\zeta)/2(\kappa^2-1)(\zeta^2+\gamma^2) \tag{19}$$

with

$$R(\zeta) = (2\zeta^2+\kappa^2)^2 - 4\zeta^2\alpha\beta \tag{20}$$

being Rayleigh's function. This function vanishes only at $\zeta = \pm i\gamma$ where γ is the ratio of the P wave velocity to the velocity of the Rayleigh surface wave for the medium and γ depends only on Poisson's ratio. For real elastic solids, $\gamma > \kappa$, so that the Rayleigh wave velocity is less than that of the shear wave. The function $K(\zeta)$ has neither poles nor zeros and as $|\zeta| \to \infty$, $|K| \to 1$. The branch points at $\zeta = \pm i$ and $\pm i\kappa$ and the zeros at $\pm i\gamma$ in $R(\zeta)$ indicate the occurrence of scattered compressional and shear waves from the tips of the crack and, in addition, Rayleigh waves will propagate back and forth along its surface.

To solve the Wiener–Hopf equation (18) we follow the technique used in Refs. [3–5]. First the function $K(\zeta)$ is factored into two functions that are analytic in the overlapping $+$ and $-$ regions as

$$K(\zeta) = K_+(\zeta)K_-(\zeta) \tag{21}$$

where

$$K_\pm(\zeta) = \exp\left\{-\frac{1}{\pi}\int_1^\kappa \tan^{-1}\left[\frac{4\eta^2(\eta^2-1)^{\frac{1}{2}}(\kappa^2-\eta^2)^{\frac{1}{2}}}{(2\eta^2-\kappa^2)^2}\right]\frac{d\eta}{\eta \mp i\zeta}\right\} \tag{22}$$

so that $K_+(\zeta) = K_-(-\zeta)$. Details for accomplishing the above factorization are given by Fredricks [7] in connection with a Wiener–Hopf problem for a half-space in contact with a fluid quarter-space. Note, however, that in [7] the K function is the reciprocal of equation (19) and the complex transform plane is rotated by 90° from our ζ-plane.

Next, we change ζ in equation (18) to $\zeta' = \xi' + i\eta'$ and divide both sides by $2\pi i D_+(\zeta')(\zeta'-\zeta)$ where

$$D_\pm(\zeta) = (\zeta \pm i)^{-\frac{1}{2}}(\zeta \pm i\gamma)K_\pm(\zeta). \tag{23}$$

The resulting equation is then integrated from $\xi' = -\infty$ to $\xi' = \infty$ along a horizontal line L_1 in the ζ'-plane located in $|\eta'| < 1$ and the point ζ is taken *above* this line. The integral of the left-hand side can be shown to be zero since the integrand is analytic below L_1 and the edge conditions at $x = 0, 1$ ensure that $|\bar{G}_E| \to 0$ sufficiently rapidly as $|\zeta'| \to \infty$ for the integral taken on an infinite semi-circle in the lower ζ'-plane to vanish. Furthermore, from the decomposition theorem for functions analytic in a strip [6], the integral of the right-hand side is a $+$ function. The result becomes

$$\bar{\Upsilon}_+(\zeta s) = \left[\frac{D_+(\zeta)}{D_+(i\cos\alpha)} - 1\right]\frac{i\Gamma_1\bar{f}}{\zeta - i\cos\alpha} - \frac{D_+(\zeta)}{2\pi i}\int_{L_1}\frac{e^{-i\zeta' s}}{D_+(\zeta')(\zeta'-\zeta)} \cdot \left[\bar{\Upsilon}_-(\zeta' s) - \frac{i\Gamma_1\bar{f}\,e^{-s\cos\alpha}}{\zeta' - i\cos\alpha}\right]d\zeta' \tag{24a}$$

where it has been assumed that the point $\zeta' = i\cos\alpha$ lies above L_1.

Similarly, we can divide equation (18), after changing ζ to ζ', by $2\pi i D_-(\zeta')(\zeta'-\zeta)\times \exp(-i\zeta' s)$ and integrate both sides from $\xi' = -\infty$ to $+\infty$ along a line L_2 lying in $|\eta'| < 1$ with the point ζ now located *below* L_2. Again, the integral of the left-hand side can be shown to be zero while the integral of the right side is a $-$ function. With the point $\zeta' = i\cos\alpha$ taken below L_2 the result is

$$\bar{\Upsilon}_-(\zeta s) = \left[1-\frac{D_-(\zeta)}{D_-(i\cos\alpha)}\right]\frac{i\Gamma_1 \bar{f}\, e^{-s\cos\alpha}}{\zeta - i\cos\alpha} + \frac{D_-(\zeta)}{2\pi i}\int_{L_2}\frac{e^{i\zeta' s}}{D_-(\zeta')(\zeta'-\zeta)} \cdot \left[\bar{\Upsilon}_-(\zeta' s) + \frac{i\Gamma_1 \bar{f}}{\zeta' - i\cos\alpha}\right] d\zeta'. \tag{24b}$$

Thus, we obtain the pair of coupled singular integral equations (24) which are typical of those occurring when the Wiener–Hopf method is applied to a problem with a finite discontinuity barrier [3–6]. As done in [3–5] we solve them by the standard iteration procedure. The first terms on the right sides of equations (24) are the "zeroth order" solutions $\bar{\Upsilon}^{(0)}_{+,-}$. Substitution of these expressions for $\bar{\Upsilon}_{+,-}$ into the integrals in equations (24) produces the "first order" solutions $\bar{\Upsilon}^{(1)}_{+,-}$, and so on. Note that by this process the "nth order" solution will be equal to the $(n-1)$th order" solution plus an integral of the $(n-1)$th solution. Remarkably, it can be shown that the inverse Laplace transform of this iteration series is always a finite one for any finite time and so an *exact solution* is obtained at any stage of iteration up to a finite value of time which increases with increasing order of iteration. This has been shown in [4, 5] and will be illustrated below for the zeroth and first order solutions.

From equations (24) the zeroth order solutions are

$$\Upsilon^{(0)}_+ = \left[\frac{D_+(\zeta)}{D_+(i\cos\alpha)} - 1\right]\frac{i\Gamma_1 \bar{f}}{\zeta - i\cos\alpha} \tag{25a}$$

$$\Upsilon^{(0)}_- = \left[1-\frac{D_-(\zeta)}{D_-(i\cos\alpha)}\right]\frac{i\Gamma_1 \bar{f}\, e^{-s\cos\alpha}}{\zeta - i\cos\alpha} \tag{25b}$$

which correspond to the exact solutions for the separate scattering of the symmetric incident P wave by the semi-infinite cracks, $0 < x$ and $x < 1$, respectively. Thus, physically, we expect that these results are exact until the P waves scattered at the crack edges interact with the opposite edges, i.e. until $t = 1+\cos\alpha$ at $x = 0$ and until $t = 1$ at $x = 1$.† This indeed will now be shown mathematically.

Substitute equations (25) into equations (24) to find the first order results,

$$\Upsilon^{(1)}_+ = \Upsilon^{(0)}_+ + \frac{D_+(\zeta)\Gamma_1 \bar{f}}{2\pi D_-(i\cos\alpha)} e^{-s\cos x}\, \alpha \int_{L_1}\frac{D_-(\zeta')\, e^{-i\zeta' s}\, d\zeta'}{D_+(\zeta')(\zeta'-\zeta)(\zeta'-i\cos\alpha)} \tag{26a}$$

$$\Upsilon^{(1)}_- = \Upsilon^{(0)}_- + \frac{D_-(\zeta)\Gamma_1 \bar{f}}{2\pi D_+(i\cos\alpha)}\int_{L_2}\frac{D_+(\zeta')\, e^{i\zeta' s}\, d\zeta'}{D_-(\zeta')(\zeta'-\zeta)(\zeta'-i\cos\alpha)}. \tag{26b}$$

† Observe from Fig. 1 that the incident P wave does not reach the edge $x = 1$ until $t = \cos\alpha$ as indicated by the shifting factor $\exp(-s\cos\alpha)$ in equation (25b).

To interpret these expressions we first deform the integration paths in equations (26a) and (26b) around the branch cuts along the η'-axis in the lower and upper ζ'-planes, respectively. With η' then changed to λ the results become,

$$\Upsilon_{+}^{(1)} = \Upsilon_{+}^{(0)} - \frac{D_{+}(\zeta)\Gamma_1 \bar{f}}{2\pi D_{-}(i\cos\alpha)} e^{-s\cos\alpha}\left[\int_1^{\infty} \frac{(\lambda^2-\kappa^2/2)^2(\lambda-1)^{\frac{1}{2}}}{(\zeta+i\lambda)(\lambda+1)^{\frac{1}{2}}} F(\lambda,\alpha)\, e^{-\lambda s}\, d\lambda + \int_{\kappa}^{\infty} \frac{\lambda^2(\lambda-1)(\lambda^2-\kappa^2)^{\frac{1}{2}}}{\zeta+i\lambda} F(\lambda,\alpha)\, e^{-\lambda s}\, d\lambda\right] \tag{27a}$$

$$\Upsilon_{-}^{(1)} = \Upsilon_{-}^{(0)} - \frac{D_{-}(\zeta)\Gamma_1 \bar{f}}{2\pi D_{+}(i\cos\alpha)}\left[\int_1^{\infty} \frac{(\lambda^2-\kappa^2/2)^2(\lambda-1)^{\frac{1}{2}}}{(\zeta-i\lambda)(\lambda+1)^{\frac{1}{2}}} F(\lambda,\pi-\alpha)\, e^{-\lambda s}\, d\lambda + \int_{\kappa}^{\infty} \frac{\lambda^2(\lambda-1)(\lambda^2-\kappa^2)^{\frac{1}{2}}}{\zeta-i\lambda} F(\lambda,\pi-\alpha)\, e^{-\lambda s}\, d\lambda\right] \tag{27b}$$

where

$$F(\lambda,\alpha) = \frac{(\lambda+\gamma)K_{+}^2(i\lambda)}{(\lambda+\cos\alpha)(\lambda-\gamma)(\lambda^2-a_1^2)(\lambda^2-a_2^2)} \tag{28}$$

and $\int$ means the Cauchy principal value integral which occurs because of the pole at $\lambda = \gamma$ along the path of integration. The constants a_1^2, a_2^2 and γ^2 are zeros of the "rationalized Rayleigh's function",

$$16(\kappa^2-1)(\lambda^2-\gamma^2)(\lambda^2-a_1^2)(\lambda^2-a_2^2) = [4\lambda^2(\lambda^2-1)^{\frac{1}{2}}(\lambda^2-\kappa^2)^{\frac{1}{2}} - (2\lambda^2-\kappa^2)^2] \cdot [4\lambda^2(\lambda^2-1)^{\frac{1}{2}}(\lambda^2-\kappa^2)^{\frac{1}{2}} + (2\lambda^2-\kappa^2)^2], \tag{29}$$

but for real materials a_1^2 and a_2^2 are, depending on the value of Poisson's ratio, either complex conjugates or real numbers less than unity. For example, with $\nu = \frac{1}{4}$, $a_1^2 = 3(3-3^{\frac{1}{2}})/4$, $a_2^2 = \frac{3}{4}$ and $\gamma^2 = 3(3+3^{\frac{1}{2}})/4$. In any case $\lambda = \gamma$ is the only singularity in the integrands in equations (27) along the path of integration.

Now we can interpret physically the first order results. The two integrals in each of equations (27) are recognized as Laplace transforms of specific functions that are zero for $t < 1$ and $t < \kappa$. Thus, in equation (27a) where they are multiplied by $\exp(-s\cos\alpha)$, these integrals represent P and S waves that arrive at the crack tip $x = 0$ at $t = 1+\cos\alpha$ and $t = \kappa+\cos\alpha$, respectively. However, these correspond precisely to the times when the first scattered P and S waves which emanate from the crack tip at $x = 1$ at $t = \cos\alpha$ will reach the opposite tip. In other words, the integrals in equations (27) represent the first interaction effects of the waves scattered from the two crack tips. In equation (27b) the integrals correspond to the P and S waves scattered at the tip $x = 0$ and which arrive at the tip $x = 1$ at $t = 1$ and $t = \kappa$, respectively. The propagation of the Rayleigh waves along the crack surfaces from one tip to the other is signified by the poles at $\lambda = \gamma$ in the integrands.

Since the P waves rescattered at each tip will not return to the opposite tip for another unit of time, we expect that the first order solutions should be exact until $t = 2$ and $t = 2+\cos\alpha$ in equations (27a) and (27b) respectively. This can be verified mathematically by substituting equations (27) back into equations (24). One obtains the first order solution plus four different double integrals that represent the rescattered waves (*PP*, *PS*, *SP*, *SS*).

Their inverse Laplace transforms can be shown to be zero until $t = 2$, $t = 1+\kappa$ (for both *PS* and *SP*), and $t = 2\kappa$, respectively. In fact, we can deduce in general that

$$\begin{aligned} \Upsilon_+^{(2n)} &= \Upsilon_+^{(2n-1)} \quad \text{for } 0 \le t \le 2n \\ \Upsilon_+^{(2n+1)} &= \Upsilon_+^{(2n)} \quad \text{for } 0 \le t \le 2n+1+\cos\alpha \end{aligned} \tag{30a}$$

and

$$\begin{aligned} \Upsilon_-^{(2n)} &= \Upsilon_-^{(2n-1)} \quad \text{for } \cos\alpha \le 2n+\cos\alpha \\ \Upsilon_-^{(2n+1)} &= \Upsilon_-^{(2n)} \quad \text{for } \cos\alpha \le t \le 2n+1 \end{aligned} \tag{30b}$$

Here, we stop at the first order solution. It will yield exact results for the stress intensities at each crack tip up to two *P* wave, crack width, transit times beyond the incident wave arrival time.

Crack-tip normal stress intensities. Observe from equations (13) that the inverse transforms of equations (27), multiplied by s, yield the normal stresses in front of the two crack tips along $y = 0$. However, since we are interested in the leading term for the stresses near the crack tips, the Fourier transform inversion [equation (15b)] need be performed only on the leading term in the expansion of equations (27) for $|\zeta| \to \infty$. Noting the definition of $D_\pm$ in equation (23) and that $|K_\pm| \to 1$ as $|\zeta| \to \infty$, we can readily show that the dominant term in each of equations (27) is proportional to $|\zeta|^{-\frac{1}{2}}$. The inverse Fourier transform of these terms becomes

$$s\bar{\tau}_0^{(1)}(x) \to \left(\frac{2s^3}{\pi|x|}\right)^{\frac{1}{2}} \Gamma_1 \bar{f}(s)\left[\frac{\cos\alpha/2}{(\gamma+\cos\alpha)K_+(i\cos\alpha)} - \frac{\sin\alpha/2\, e^{-s\cos\alpha}\bar{J}_1(\alpha)}{2\pi(\gamma-\cos\alpha)K_-(i\cos\alpha)}\right] \tag{31a}$$

as $x \to 0^-$ and

$$s\bar{\tau}_1^{(1)}(x-1) \to \left(\frac{2s^3}{\pi(x-1)}\right)^{\frac{1}{2}} \Gamma_1 \bar{f}(s)\left[\frac{\sin\alpha/2\, e^{-s\cos\alpha}}{(\gamma-\cos\alpha)K_-(i\cos\alpha)} - \frac{\cos\alpha/2\bar{J}_1(\pi-\alpha)}{2\pi(\gamma+\cos\alpha)K_+(i\cos\alpha)}\right] \tag{31b}$$

as $x \to 1^+$. Of course, we recall that $\bar{\tau}_0(x) = 0$ for $x > 0$ and $\bar{\tau}_1(x-1) = 0$ for $x < 1$. In equations (31)

$$\bar{J}_1(\alpha) = \int_1^\infty (\lambda^2-\kappa^2/2)^2\left(\frac{\lambda-1}{\lambda+1}\right)^{\frac{1}{2}} F(\lambda,\alpha)\, e^{-\lambda s}\, d\lambda + \int_\kappa^\infty \lambda^2(\lambda-1)(\lambda^2-\kappa^2)^{\frac{1}{2}} F(\lambda,\alpha)\, e^{-\lambda s}\, d\lambda \tag{32}$$

where $F(\lambda,\alpha)$ was defined by equation (28).

Since the inverse Laplace transform of equation (32), $J_1(t,\alpha)$, is obtained by inspection, the inverse Laplace transforms of equations (31) are readily found in terms of convolution integrals. Details are presented for the particular case where

$$f(t) = \tfrac{1}{2}t^2, \qquad (s) = \frac{1}{s^3}. \tag{33}$$

Then the stresses associated with the incident wave (6) approach the uniform static values, as $t \to \infty$,

$$\tau_{xx} = \Gamma_0, \qquad \tau_{yy} = \Gamma_1, \qquad \tau_{xy} = \Gamma_2 \tag{34}$$

where $\Gamma_{0,1,2}$ are the coefficients of f in equations (6).

Now, it is well known [8] that the leading term for the static normal stress at each crack tip produced by the loading (34) becomes for our geometry (Fig. 1),

$$\tau_{yy}(x,0) \to \frac{\Gamma_1}{2|x|^{\frac{1}{2}}} \quad \text{as } x \to 0^- \tag{35a}$$

$$\tau_{yy}(x-1,0) \to \frac{\Gamma_1}{2(x-1)^{\frac{1}{2}}} \quad \text{as } x \to 1^+ \tag{35b}$$

Hence, we define the "normalized dynamic stress-intensity factors" by dividing equations (31a) and (31b) by equations (35a) and (35b), respectively. The inverse Laplace transform of the result is denoted by $K_I(0 \text{ or } 1, t)$ corresponding to the crack tip at $x = 0$ or 1, respectively. For large times we expect $K_1 \to 1$.

Noting that the inverse Laplace transform of $s^{-\frac{1}{2}}$ is $2(t/\pi)^{\frac{1}{2}}$ and performing the aforementioned steps, we obtain the first order results:

$$K_1^{(1)}(0,t) = 2^{\frac{1}{2}}\left(\frac{4}{\pi}\right)\left[\frac{t^{\frac{1}{2}}\cos\alpha/2}{(\gamma+\cos\alpha)K_+(i\cos\alpha)} - \frac{\sin\alpha/2\,(t-\cos\alpha)^{\frac{1}{2}} * J_1(t,\alpha)}{2\pi(\gamma-\cos\alpha)K_-(i\cos\alpha)}H(t-\cos\alpha)\right] \tag{36a}$$

$$K_1^{(1)}(1,t) = 2^{\frac{1}{2}}\left(\frac{4}{\pi}\right)\left[\frac{(t-\cos\alpha)^{\frac{1}{2}}\sin\alpha/2}{(\gamma-\cos\alpha)K_-(i\cos\alpha)}H(t-\cos\alpha) - \frac{\cos\alpha/2\,t^{\frac{1}{2}} * J_1(t,\pi-\alpha)}{2\pi(\gamma+\cos\alpha)K_+(i\cos\alpha)}\right] \tag{36b}$$

where $H(t)$ is the unit step function and $*$ denotes the convolution operation,

$$f * g \equiv \int_0^t f(t-\lambda)g(\lambda)\,d\lambda.$$

Thus, for example,

$$t^{\frac{1}{2}} * J_1(t,\pi-\alpha) = H(t-1)\int_1^t (t-\lambda)^{\frac{1}{2}}(\lambda^2-\kappa^2/2)^2\left(\frac{\lambda-1}{\lambda+1}\right)^{\frac{1}{2}} F(\lambda,\pi-\alpha)\,d\lambda$$

$$+H(t-\kappa)\int_\kappa^t (t-\lambda)^{\frac{1}{2}}\lambda^2(\lambda-1)(\lambda^2-\kappa^2)^{\frac{1}{2}}F(\lambda,\pi-\alpha)\,d\lambda. \tag{37}$$

Note that for $t < \gamma$, the pole at $\lambda = \gamma$ in $F(\lambda, \pi-\alpha)$ lies outside the above integration intervals and the integrals are actually conventional. However, for $t > \gamma$ the pole falls within the range of integration and the Cauchy principal values must be taken. Thus, the arrival of the Rayleigh wave at each crack tip is indicated by the change in the form of the convolution integrals in equations (36).

Numerical calculations of equations (36) are presented and discussed in Section 5 along with similar ones for the normalized shear stress intensity factors which are derived below.

(b) *Anti-symmetric problem*

In the anti-symmetric problem, u and τ_{yy} are odd functions of y and so they vanish at $y = 0$ for $x < 0$ and $x > 1$. Furthermore, the incident wave [equation (9) with the lower sign] produces zero normal stress at $y = 0$ and the shear stress

$$\tau_{xy}^{(i)}(x, 0, t) = \Gamma_2 \dot{f}(t - x\cos\alpha) \tag{38}$$

Thus, by introducing unknown functions for $u^{(s)}$ in $0 < x < 1$ and $\tau_{xy}^{(s)}$ in $x < 0$ and $x > 1$ along the boundary of the half-space, $y > 0$, we can again extend the boundary conditions (7) to

$$u^{(s)}(x, 0^+, t) = \begin{cases} \kappa^2 p(x, t)/2(\kappa^2 - 1) & \text{for } 0 < x < 1 \\ 0 & \text{otherwise} \end{cases} \tag{39a}$$

$$\tau_{yy}^{(s)}(x, 0, t) = 0 \qquad \text{for all } x \tag{39b}$$

$$\tau_{xy}^{(s)}(x, 0, t) = \begin{cases} \dot{q}_0(x, t) & \text{for } x < 0 \\ -\Gamma_2 \dot{f}(t - x\cos\alpha) & \text{for } 0 < x < 1 \\ \dot{q}_1(x - 1, t) & \text{for } 1 < x \end{cases} \tag{39c}$$

At this point the analysis proceeds exactly along the lines described in (a) above for the symmetric problem and we are lead to the generalized Wiener–Hopf equation

$$-\bar{P}_E \beta^{-1}(\zeta^2 + \gamma^2)K(\zeta) = \bar{Q}_+ + e^{-i\zeta s}\bar{Q}_- + \frac{i\Gamma_2 \bar{f}}{\zeta - i\cos\alpha}(1 - e^{-s\cos\alpha - i\zeta s}) \tag{40}$$

where $\bar{Q}_\pm$ are the Fourier and Laplace transforms of q_0 and q_1, respectively, and $K(\zeta)$ was defined by equation (19).

Note that equation (40) is the same as the previous generalized W–H equation (18) except that β appears on the left side of (40) instead of α. Of course there are the obvious changes from Γ_1 to Γ_2 and in the symbols for the unknown $+$, $-$ and E functions.

Therefore, we shall omit all the remaining details of analysis leading to the first order results for the shear stress intensity factors. In fact, by replacing $\zeta \pm i$ by $\zeta \pm i\kappa$ in the expression for $D_\pm$ in equation (23), the first order solution of equation (40) is immediately obtained from equations (26). Thereafter, the algebraic calculations become slightly different, but the procedures are identical to those in (a). We obtain the leading terms for the shear stresses at the crack tips as

$$s\bar{q}_0^{(1)}(x) \to \left(\frac{s^3}{\pi|x|}\right)^{\frac{1}{2}} \Gamma_2 \bar{f}(s)\left[\frac{(\kappa + \cos\alpha)^{\frac{1}{2}}}{(\gamma + \cos\alpha)K_+(i\cos\alpha)} - \frac{(\kappa - \cos\alpha)^{\frac{1}{2}} e^{-s\cos\alpha}\bar{J}_2(\alpha)}{2\pi(\gamma - \cos\alpha)K_-(i\cos\alpha)}\right] \tag{41a}$$

as $x \to 0^-$ and

$$s\bar{q}_1^{(1)}(x - 1) \to \left(\frac{s^3}{\pi(x-1)}\right)^{\frac{1}{2}} \Gamma_2 \bar{f}(s)\left[\frac{(\kappa - \cos\alpha)^{\frac{1}{2}} e^{-s\cos\alpha}}{(\gamma - \cos\alpha)K_-(i\cos\alpha)}\right.$$

$$\left. - \frac{(\kappa + \cos\alpha)^{\frac{1}{2}}\bar{J}_2(\pi - \alpha)}{2\pi(\gamma + \cos\alpha)K_+(i\cos\alpha)}\right] \quad \text{as } x \to 1^+ \tag{41b}$$

where

$$\bar{J}_2(\alpha) = \int_1^\infty \lambda^2(\lambda-\kappa)(\lambda^2-1)^{\frac{1}{2}} F(\lambda,\alpha)\,e^{-\lambda s}\,d\lambda + \int_\kappa^\infty (\lambda^2-\kappa^2/2)^2\left(\frac{\lambda-\kappa}{\lambda+\kappa}\right)^{\frac{1}{2}} F(\lambda,\alpha)\,e^{-\lambda s}\,d\lambda \tag{42}$$

and $F(\lambda, \alpha)$ was defined by equation (28).

The above expressions contain the dynamic shear stress intensity factors for an arbitrary incident P wave profile. However, when $f(t) = (\frac{1}{2})t^2$ which produces in the long-time limit, the static loading (34), we can normalize equations (41) by the known [8] static shear stresses at the crack tips,

$$\tau_{xy}(x,0) \to \frac{\Gamma_2}{2|x|^{\frac{1}{2}}} \qquad \text{as } x \to 0^- \tag{43a}$$

$$\tau_{xy}(x-1,0) \to \frac{\Gamma_2}{2(x-1)^{\frac{1}{2}}} \quad \text{as } x \to 1^+ \tag{43b}$$

and thereby define the "normalized dynamic shear stress intensity factors" K_{II} (0 or 1, t). We obtain the results

$$K_{II}^{(1)}(0,t) = \frac{4}{\pi}\left\{\frac{[(\kappa+\cos\alpha)t]^{\frac{1}{2}}}{(\gamma+\cos\alpha)K_+(i\cos\alpha)} - \frac{[(\kappa-\cos\alpha)(t-\cos\alpha)]^{\frac{1}{2}} * J_2(t,\alpha)}{2\pi(\gamma-\cos\alpha)K_-(i\cos\alpha)}\,H(t-\cos\alpha)\right\} \tag{44a}$$

$$K_{II}^{(1)}(1,t) = \frac{4}{\pi}\left\{\frac{[(\kappa-\cos\alpha)(t-\cos\alpha)]^{\frac{1}{2}}}{(\gamma-\cos\alpha)K_-(i\cos\alpha)}\,H(t-\cos\alpha) - \frac{[(\kappa+\cos\alpha)t]^{\frac{1}{2}} * J_2(t,\pi-\alpha)}{2\pi(\gamma+\cos\alpha)K_+(i\cos\alpha)}\right\} \tag{44b}$$

where $J_2(t, \alpha)$ is found from equation (42) by inspection.

Note that Γ_2 [$=\sin 2\alpha$; cf. equations (6) and (34)] vanishes when $\alpha = \pi/2$, which is the case of perpendicular incidence. Thus, both the static and dynamic shear stress intensity factors are zero in this case and their ratio, while non-zero, appears to be physically meaningless. However, for the problem of a normally incident SV wave, i.e.

$$\phi^{(i)} = 0, \qquad \psi^{(i)} = \tfrac{1}{2}(t-\kappa y)^2$$

neither the dynamic, nor analogous static, shear stress intensity factors are zero and their ratio happens to be equal to the expressions in (44) with $\alpha = \pi/2$. In other words, equations (44) are significant for all values of α in $0 < \alpha \leq \pi/2$, but at $\alpha = \pi/2$ their significance is attached to a different problem.

4. SEPARATION OF CRACK SURFACES

In the foregoing analysis it has been assumed that the top and bottom surfaces of the crack are always kept separated. For otherwise, at the instant and at points where the crack surfaces closed, the boundary conditions (7) would be invalid and would have to be changed to specify continuity of the vertical displacement and normal stress along the crack and, in the case of smooth surfaces, zero shear stress. A continual separation of the surfaces could be achieved by imposing a static tension in the y-direction of sufficient magnitude to prevent the crack from closing during the dynamic events. Alternatively, one could use the crack model as an approximation to a thin elliptical cavity whose surfaces remained separated even when our solution might predict that the line crack would close. However,

in the former situation, the stress intensity factors obtained here would be incomplete, as an additional static field would exist; while in the latter case, our results would only be approximate.

Therefore, we are interested to know whether the crack will actually remain open under the action of the incident wave (33) which produces a tension in the y-direction (6) and thus initially separates the crack surfaces. Papadopoulos [9] has found that for a tensile wave, incident upon a semi-infinite crack, the surfaces still would close after the diffracted Rayleigh wave has passed. Also, for an oscillating incident wave, such as the plane harmonic wave considered by Sih and Loeber it was pointed out that the finite crack would open and close in cyclic fashion and so a static tension would have to be imposed [1]. In our problem, however, it is not apparent that either of the above findings are duplicated. Certainly the harmonic wave results are not applicable. Furthermore, while we observe that the finite crack *tends* to close in the wake of the first scattered Rayleigh waves, it is found that before the crack can *actually* close, the second series of scattered waves will have been generated and these may very well keep the surfaces separated.

To calculate the relative displacement between the crack surfaces, i.e. $\kappa^2 g(x,t)/(\kappa^2-1) \equiv h(x,t)$, we use equations (11a) and (18). Substitution of $\bar{\Upsilon}_+^{(n)}$ and $\bar{\Upsilon}_-^{(n)}$ into equation (18) yields $\bar{G}_E^{(n)}$ from which $h^{(n)}(x,t)$ can be calculated by inversion of the transforms and which will be an exact result for a finite time. Unfortunately, we have found it so far too complicated to obtain $h^{(1)}(x,t)$ which would cover the time period during which the stress intensity factor results are exact. This is because the inverse Fourier transform of $\bar{G}_E^{(1)}$ cannot be performed easily and in closed form as was the case for $\bar{\Upsilon}_\pm^{(1)}$ when we considered only the leading term for the stresses at the crack edges. Therefore, we examine the zeroth order solution $h^{(0)}(x,t)$ which will be exact at a point x along the crack until the first rescattered P wave arrives, i.e. at the smaller of the times $1+\cos\alpha+x$ and $2-x$. These are the arrival times for the rescattered P waves which originated at the edges $x=1$ and $x=0$, respectively.

Details for obtaining $h^{(0)}(x,t)$ consist of substituting equations (25) into (18); inverting the Fourier transform for $\bar{G}_E^{(0)}$ which includes deforming the integration paths around appropriate branch cuts in the ζ-plane; and then inverting the Laplace transform by the convolution theorem. Equation (45) below is the result when $f(t)=t^2/2$ and $\alpha=\pi/2$, i.e. the case of normal incidence.

$$h^{(0)}(x,t) = 2t+\frac{3}{2\pi}[H(t-x)I_1(t,x)+H(t-\kappa x)I_2(t,x) + H(t-1+x)I_1(t,1-x)+H(t-\kappa+\kappa x)I_2(t,1-x)] \tag{45}$$

where

$$I_1(t,x) = \int_1^{t/x} (\eta^2-\kappa^2/2)^2 M(t,x,\eta)\frac{d\eta}{\eta} \tag{46a}$$

$$I_2(t,x) = \int_\kappa^{t/x} \eta(\eta^2-1)^{\frac{1}{2}}(\eta^2-x^2)^{\frac{1}{2}} M(t,x,\eta)\,d\eta \tag{46b}$$

with

$$M(t,x,\eta) = \frac{(t-\eta x)(\eta-1)^{\frac{1}{2}}K_+(i\eta)}{(\eta^2-a_1^2)(\eta^2-a_2^2)(\gamma-\eta)}. \tag{47}$$

The first term in equation (45) represents the effect of the incident tensile wave and its reflection from the bottom surface of the crack. The integrals I_1 and I_2 represent the first scattered P and S waves, respectively, that emanate from $x = 0$ and 1, while the scattered Rayleigh waves are again indicated by the change of I_1 and I_2 to principal value integrals when their upper limits exceed γ. If we delete the integrals with argument $1-x$, we obtain the exact solution for a semi-infinite crack along the positive x-axis. Thus, we observe Papadopoulos' finding that this crack will eventually close after the Rayleigh wave passes [9]. This is because I_1 and I_2 become negative when their upper limits exceed γ† and an asymptotic analysis of these integrals for large time shows that they decrease faster than $2t$ and so will dominate the leading positive term in (45). However, for the finite crack, we can interpret equation (45) only for $t < 1+x$ when $0 < x < \frac{1}{2}$. (Because of the symmetry, when $\alpha = \pi/2$, we only treat half of the crack.) Beyond this time the rescattered waves must be included.

Numerical results for $h^{(0)}(x, t)$ are plotted vs. time for different values of x in Fig. 2. The integrals in equation (45) were evaluated by a similar technique to that described in the Appendix for the integrals in equations (36) and (44). Note that the crack stays open during the passage of the first series of scattered waves across its width. Of course in the long time limit the crack will be opened since the field becomes one of uniform static tension (34). However, further calculations are required to determine whether the finite crack will indeed stay open during the time period in between, thus making it unnecessary to superimpose a field of static tension.

To determine the jump in the vertical displacement in physical units the ordinates in Fig. 2 must be multiplied by $l\tau_0/\mu$ where l is the actual crack width, $\kappa^2\tau_0$ is the normal stress associated with the incident wave and μ is the shear modulus of the medium.

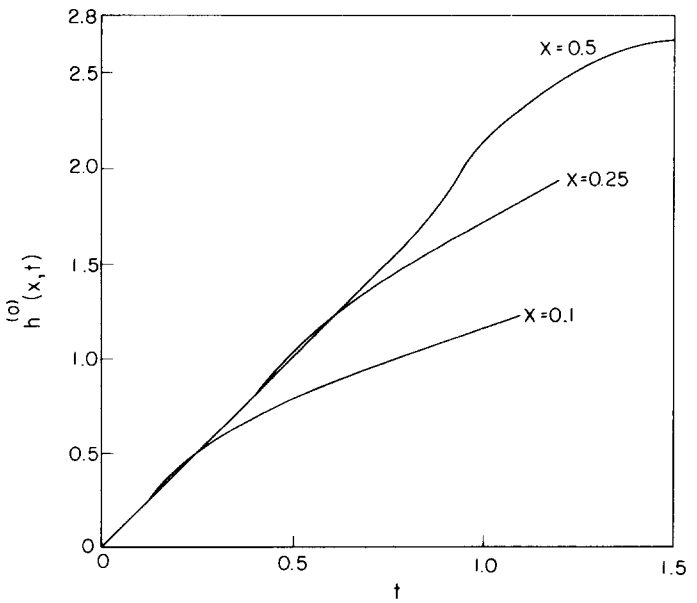

FIG. 2. Magnitude of vertical separation of crack surfaces $h^{(0)}$ vs. time at various points x along crack for $\alpha = 90°$ and $\nu = \frac{1}{4}$.

† Note that in the integrands in (46) $K_+(in)$ is positive and both a_1 and a_2 are less than unity. Thus for $t/x < \gamma$, I_1 and I_2 in (46) are positive.

5. NUMERICAL RESULTS FOR INTENSITY FACTORS

The time variations of the crack-tip, stress intensity factors are shown in Figs. 3 and 4 for various angles of incidence and Poisson's ratio $\nu = \frac{1}{4}$. This yields $\kappa = 3^{\frac{1}{2}}$ and $\gamma = 1{\cdot}8839$.

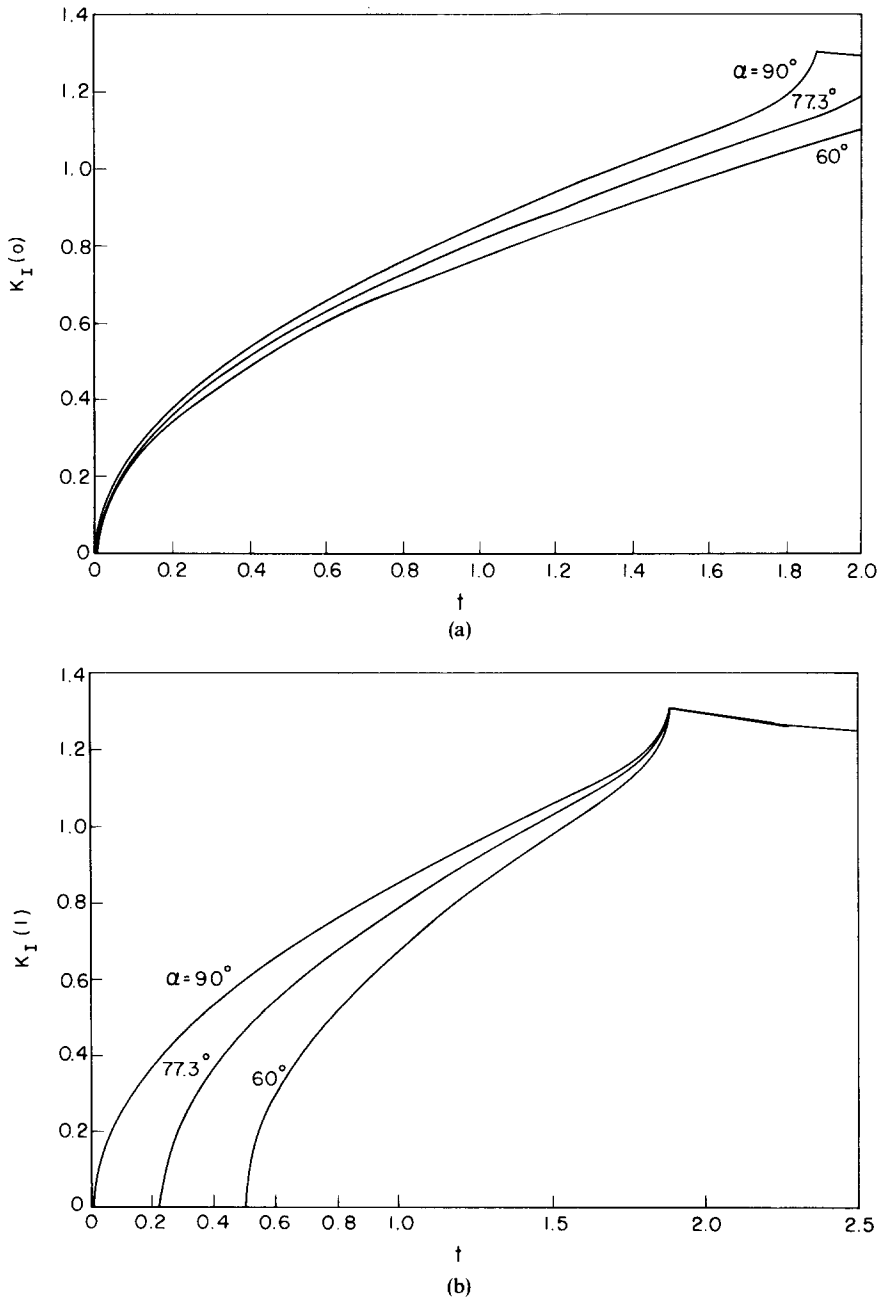

FIG. 3. Normalized normal stress intensity factors K_I vs. time for various values of α and $\nu = \frac{1}{4}$. (a) Intensity factors at $x = 0$, (b) intensity factors at $x = 1$.

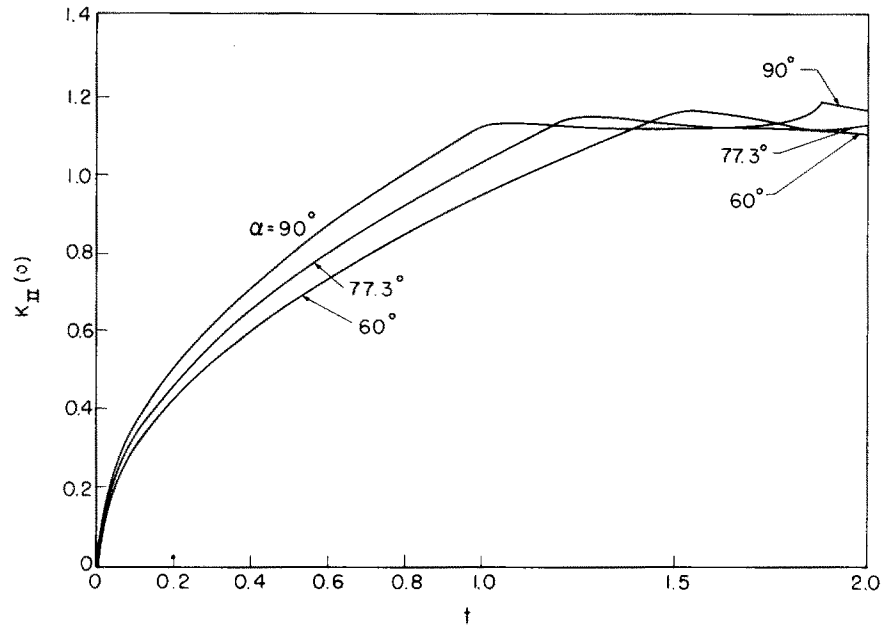

(a)

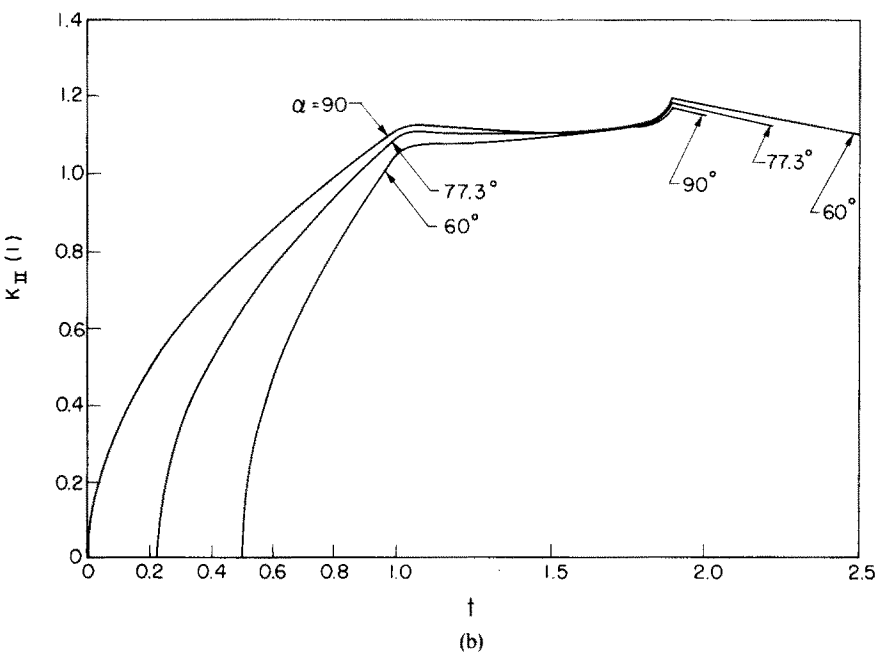

(b)

FIG. 4. Normalized shear stress intensity factors K_{II} vs. time for various values of α and $\nu = \frac{1}{4}$. (a) Intensity factors at $x = 0$, (b) intensity factors at $x = 1$.

By following the procedure described in the Appendix for evaluating the principal value integrals in equations (36) and (44), we were able not only to perform accurate numerical calculations, but also were successful in extracting analytically the contributions of the scattered Rayleigh waves. By so doing we are able to show that the maximum dynamic intensity factors occur exactly at the instant of arrival of the scattered Rayleigh wave from the opposite crack tip, provided that this event is realized before the rescattered P wave returns to the tip of interest, i.e. before the period of validity of our solution expires.

For example, at $x = 0$ the first scattered Rayleigh wave from $x = 1$ arrives at $t = \gamma + \cos\alpha$ and the second scattered P wave returns at $t = 2$. Thus, only when $\gamma + \cos\alpha < 2$ ($\alpha > 83{\cdot}3°$) are the maximum dynamic intensities found from the "first order" solution [cf. Figs. 3(a) and 4(a)]. On the other hand, at $x = 1$ the first Rayleigh wave arrival is at $t = \gamma$ for any angle of incidence and there our solution is exact up to $t = 2 + \cos\alpha$. Hence, we always find the peak intensity factors at this edge [cf. Figs. 3(b) and 4(b)].

To see that the peak intensity factors occur at $t = \gamma$ at $x = 1$ (or $t = \gamma + \cos\alpha$ at $x = 0$) we consider the expression derived for the integral in the Appendix. It is the sum of a continuously differentiable function of t at $t = \gamma$ plus a non-differentiable function proportional to $(\gamma - t)^{\frac{1}{2}} H(\gamma - t)$. Noting the minus sign before the integrals in equations (36) and (44), we see therefore that the slopes of the intensity factors will approach $+\infty$ as $t \to \gamma^-$. Furthermore, since the non-differentiable function vanishes for $t > \gamma$, it is easily seen that the intensity factors have a finite slope at $t = \gamma^+$ which is found numerically to be negative. Hence the intensity factors peak at $t = \gamma$ and the computer calculations show that these peaks are the absolute maximum values in the time intervals treated.

The maximum normal stress intensity factor is found to be about 1·30 which agrees closely with the value reported by Sih and Loeber for an incident harmonic P wave [1]. Interestingly, there is hardly any change in the peak value with angle of incidence at $x = 1$ as seen in Fig. 3(b). At $x = 0$, the peak value occurs after $t = 2$ for the acute angles of incidence considered. For $\alpha = 77{\cdot}3°$ the second scattered P wave arrives before the first scattered Rayleigh wave, while at 60° it arrives ahead of both the first scattered Rayleigh and shear waves.

The shear stress intensity factors, shown in Figs. 4, exhibit relative maxima shortly after the first scattered P wave arrives and then they reach absolute peaks at the Rayleigh wave arrival time. These peak values increase very slowly with decreasing angle of incidence, as seen in Fig. 4(b), remaining near 1·2. Recall that the shear intensity factors at 90° are for an incident SV wave and they are normalized by the equivalent static factor for that problem. In this case the peak value is found to be 1·18 which agrees closely with the result of Sih and Loeber for a normally incident harmonic SV wave [1].

6. SUMMARY AND CLOSURE

The maximum dynamic stress intensity factors have been found to exceed the analogous static values by 30 per cent for the normal crack-tip stress and by 20 per cent for the shear stress. These results occur at the instant of arrival of the first scattered Rayleigh wave from the opposite crack tip.

Since our solution is valid only during the first time period for a P wave to twice traverse the width of the crack, it is not possible to show here whether or not these peak values are indeed the maximum ones for all subsequent time. However, there are evidences that they actually are. First, the analogous harmonic wave results of Sih and Loeber [1]

predict the same maximum values. Hence, after the incident P wave, with its constant stress profile, has traveled two crack widths past the crack, it is not expected that a later relative maximum intensity factor would exceed the initial peak value and the one found from the steady-state response. Next, previous experience with transient wave interaction problems, in which the scattered waves propagate steadily outward to infinity and thus continuously remove energy from the vicinity of the obstacle, indicates that decaying responses with time are typical. These may or may not oscillate about a limiting value. Finally, and in keeping with the previous remarks, Ravera and Sih [10] have found the moderate to long time transient solution for a finite crack problem involving SH waves; and their result shows the normalized stress intensity factor oscillating with a decaying amplitude about the static limit as t increases.

REFERENCES

[1] G. C. SIH and J. F. LOEBER, Wave propagation in an elastic solid with a line of discontinuity or finite crack. *Q. appl. Math.* **27**, 193–213 (1969).
[2] J. F. LOEBER and G. C. SIH, Diffraction of antiplane shear waves by a finite crack. *J. acoust. Soc. Am.* **44**, 90–98 (1968).
[3] S. A. THAU and I. H. LU, Diffraction of transient horizontal shear waves by afinite crack and a finite rigid ribbon. *Int. J. Engng Sci.* **8**, 857–874 (1970).
[4] B. V. KOSTROV, Motion of a rigid strip-mass soldered into an elastic medium, excited by a plane wave. *PMM* **28**, 113–126 (1964).
[5] L. M. FLITMAN, On the motion of a rigid strip mass lying on an elastic half-space and excited by a seismic wave. *PMM* **26**, 1582–1604 (1963).
[6] B. NOBLE, *Methods Based on the Wiener–Hopf Technique*. Pergamon Press (1958).
[7] R. W. FREDRICKS, Diffraction of an elastic pulse in a loaded half-space. *J. acoust. Soc. Am.* **33**, 17–22 (1961).
[8] G. C. SIH, P. C. PARIS and F. ERDOGAN, Crack-tip stress intensity factors for plane extension and plate bending problems. *J. appl. Mech.* **29**, 306–312 (1962).
[9] M. PAPADOPOULOS, Diffraction of plane elastic waves by a crack, with application to a problem of brittle fracture. *J. Aust. math. Soc.* **3**, 325–339 (1963).
[10] R. J. RAVERA and G. C. SIH, Transient analysis of stress waves around cracks under antiplane strain. *J. acoust. Soc. Am.* **47**, 875–881 (1970).

APPENDIX

To calculate accurately the principal value integrals occurring in equations (36) and (44) we found it useful first to replace $K_+^2(i\lambda)$ in the integrands by the rational function approximation,

$$K_+^2(i\lambda) \approx \frac{\alpha_0+\alpha_1 h+\alpha_2\lambda^2}{\beta_0+\lambda} \tag{A1}$$

with $\alpha_0 = 1{\cdot}03066146$, $\alpha_1 = 0{\cdot}9994148$, $\alpha_2 = 0{\cdot}00006683$ and $\beta_0 = 1{\cdot}62566276$. This function agrees with the exact one calculated from equation (22) to six decimal places in $1 \leq \lambda \leq 2{\cdot}5$ which is the maximum range of values required for our calculations. Then each of the integrals can be expressed in the general form:

$$I(t) = \int_b^t \left(\frac{\lambda+b}{\lambda-b}\right)^{\frac{1}{2}} (t-\lambda)^{\frac{1}{2}} \frac{S(\lambda)}{\lambda-\gamma}\,\mathrm{d}\lambda \quad (t > b) \tag{A2}$$

where b is either unity or κ and $S(\lambda)$ is a rational function whose poles do not lie in the interval of integration for any $t > b$.

Using the identity

$$(\lambda+b)^{\frac{1}{2}} = \frac{\lambda-\gamma}{(\lambda+b)^{\frac{1}{2}}+(\gamma+b)^{\frac{1}{2}}}+(\gamma+b)^{\frac{1}{2}} \tag{A3}$$

we may write $I(t)$ as

$$I(t) = \int_b^t \left(\frac{t-\lambda}{\lambda-b}\right)^{\frac{1}{2}} \frac{S(\lambda)\,\mathrm{d}\lambda}{(\lambda+b)^{\frac{1}{2}}+(\gamma+b)^{\frac{1}{2}}}+(\gamma+b)^{\frac{1}{2}}J(t) \tag{A4}$$

where

$$J(t) = \int_b^t \left(\frac{t-\lambda}{\lambda-b}\right)^{\frac{1}{2}} \frac{S(\lambda)}{\lambda-\gamma}\,\mathrm{d}\lambda. \tag{A5}$$

The substitution $\lambda-b = u^2$ renders the first integral in (A4) a proper one of a finite function that is easily evaluated by the computer. The second integral, $J(t)$, can be evaluated in closed form as follows:

We suppose that for large λ, $S(\lambda)$ has the asymptotic expansion

$$S(\lambda) \sim A_2\lambda^2+A_1\lambda+A_0+0(\lambda^{-1}) \tag{A6}$$

where A_0, A_1 and A_2 are found explicitly by long division.† Then we define

$$T(\lambda) = S(\lambda)-A_2\lambda^2-A_1\lambda \tag{A7}$$

and note that T has the same poles and same residues at them as S and that $T \sim A_0$ as $\lambda \to \infty$. Substituting (A7) into (A5) and using the relation

$$\frac{A_2\lambda^2+A_1\lambda}{\lambda-\gamma} = A_2(\lambda+\gamma)+A_1+\frac{A_2\gamma^2+A_1\gamma}{\lambda-\gamma} \tag{A8}$$

yields

$$J(t) = \int_b^t [A_2(\lambda+\gamma)+A_1]\left(\frac{t-\lambda}{\lambda-b}\right)^{\frac{1}{2}}\mathrm{d}\lambda+\int_b^t [T(\lambda)+A_2\gamma^2+A_1\gamma]\left(\frac{t-\lambda}{\lambda-b}\right)^{\frac{1}{2}}\frac{\mathrm{d}\lambda}{\lambda-\gamma}. \tag{A9}$$

The first integral in (A9) can be reduced to an elementary one by the substitution $(\lambda-b)/(t-b) = \sin^2\theta$ and then evaluated in closed form. The second one, denoted by $L(t)$, say, can be determined from the contour integral,

$$\Lambda(t) = \frac{1}{2\pi i}\int_C [T(z)+A_2\gamma^2+A_1\gamma]\left(\frac{z-t}{z-b}\right)^{\frac{1}{2}}\frac{\mathrm{d}z}{z-\gamma} \tag{A10}$$

where C consists of a circle Γ of infinite radius, traversed in the counterclockwise sense, and a "dumbell" contour D around the branch cut between $z = b$ and $z = t$, traversed in the clockwise sense as shown in Fig. 5. When $\gamma > t$ the contour C encloses a pole at $z = \gamma$; when $\gamma < t$ the dumbell path D must encircle the point $z = \gamma$, but the residue

† In no case encountered here does $S(\lambda)$ increase more rapidly than λ^2 for large λ. In some, A_2 or A_1 and A_2 are zero.

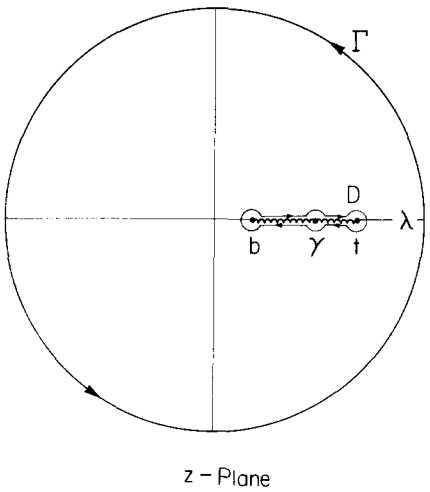

FIG. 5. Contour for integral $\Lambda(t)$ for case $t > \gamma$. For $\gamma > t$ the paths along the branch cut are unbroken straight lines. Poles of $S(z)$ are not indicated.

contributions from the upper and lower semi-circles will cancel. The integral along Γ itself, where $z = R\,e^{i\theta}$ with $R \to \infty$, can be shown to equal $(A_0 + A_1\gamma + A_2\gamma^2)$ and the integral along D is equal to $L(t)/\pi$. Therefore, by Cauchy's formula we find

$$\frac{1}{\pi} L(t) = S(\gamma)\left(\frac{\gamma - t}{\gamma - b}\right)^{\frac{1}{2}} H(\gamma - t) - (A_0 + A_1\gamma + A_2\gamma^2) + \sum \text{residues of } \frac{S(z)}{z-\gamma}\left(\frac{z-t}{z-b}\right)^{\frac{1}{2}} \text{ at poles of } S(z). \tag{A11}$$

In (A11) we have replaced T by S from equation (A7).

Note that the first term in equation (A11) represents the effect of the Rayleigh wave since it vanishes precisely at $t = \gamma$ and provides an infinite slope for $I(t)$ for $t = \gamma^-$, but not for $t = \gamma^+$. It can, in fact, be shown that the slope of $I(t)$ changes sign at $\gamma = t$ and therefore I attains a peak value at this time.

(*Received* 7 *August* 1970)

Абстракт—Исследуется отражение плоской волны расширения, произвольного профиля, от конечной линейной щели, в бесконечной упругой среде, при помощи обобщенного способа Винера-Хопфа. Составляются выражения, в явном виде, для факторов интенсивности динамических нормальных напряжений и напряжений сдвига, для каждого края щели, представленные в качестве функций времени, угла падения и числа Пуассона. Эти результаты оказываются точными в момент, когда ударяющая волна доходит до заданного края, пока как отраженная волна достигает противоположенного края, отражается снова и затем возвращается к первоначальному краю, то есть в течение время перехода ширины щели двух продольных волн. Даются численные результаты для ударяющей волны в виде скачко-образной функции напряжения, для разных углов падения. Находится, что максимальная интенсивность нормальных напряжений оказывается на 30% больше, чем аналогический стимический фактор. Величина скачка, в вертикальном перемещении вершины щели, решается для случая нормального падения, в течение времени перехода единственной продольной волны щель, в это время, остается открытой.